Electronic Supplementary Material (ESI) for Polymer Chemistry.

Supporting Information

Preparation of compressible polymer monoliths that contain mesopores capable of rapid oil–water separation

Ji Ae Chae,[a] Yuree Oh,[a] Hea Ji Kim,[a] Go Bong Choi,[a] Kyoung Min Lee,[a,b] Doyoung Jung,[a] Yoong Ahm Kim,[a] and Hyungwoo Kim*[a]

[a] School of Polymer Science and Engineering & Alan G. MacDiarmid Energy Research Institute, Chonnam National University, 77 Yongbong-ro, Buk-gu, Gwangju 61186, Korea
[b] Department of Materials Science and Engineering, Seoul National University, 1 Gwanak-ro, Gwanak-gu, Seoul 08826, Korea

*Corresponding author e-mail: kimhw@jnu.ac.kr

Contents

General Experimental

All reactions were performed in flame-dried glassware under a positive pressure of nitrogen unless otherwise noted. 1,3,5-Triethynylbenzene (**1**) was synthesized following the previous method.[S1]

Instrumentation

Proton nuclear magnetic resonance (^{1}H NMR) spectra were recorded using Bruker 400 MHz NMR spectrometers at 25 ℃. Proton chemical shift are expressed in part per million (ppm, δ scale) and are referenced to tetramethylsilane ($(CH_3)_4Si$ 0.00 ppm) or to residual protium in the solvent ($CDCl_3$, δ 7.26 ppm).

Solid-state ^{13}C CP/MAS NMR spectrum was recorded on a 500 MHz Bruker Avance III HD spectrometer (125 MHz) equipped with a CP-MAS probe.

Nitrogen adsorption–desorption isotherms were measured at 77 K by using a Belsorp-Max (BEL Japan, Inc.) apparatus. Samples were degassed at 150 ℃ under vacuum

for at least 12 h before measurements, and ultra-high purity grade nitrogen gas was used for all measurements. The specific surface area was calculated by Brunauer–Emmett–Teller (BET) method and the pore size distribution was estimated according to the nonlocal density function theory (NLDFT) with a slit model. Total pore volumes were calculated at a relative pressure of $P/P_0 = 0.990$.

Uniaxial compressive tests were performed using a universal testing machine (UTM) (MCT-2150, A&D, Japan) with a 500-N load cell at 25 ℃ in air. The cylindrical samples were compressed at a rate of 10 mm min^{-1} and triplicated during the measurement. Then, stress–strain curves were recorded. Young's modulus was obtained from the initial slope of the stress-strain curve in the strain range of 0–10%.

Micromorphology of dried hydrogels was observed using a Carl Zeiss SUPRA 55VP scanning electron microscope (SEM) at an accelerating voltage of 2 kV. Before the measurement, the sample was dried in vacuum and coated with a thin platinum layer.

Photoluminescence spectra were measured using a Shimadzu RF-5301PC spectrofluorometer.

Attenuated total reflectance Fourier-transform infrared spectroscopy (ATR-FTIR) was performed using IFS66/S (Bruker) was used to observe absorption spectra of hydrogels.

Water Contact angle measurements were conducted using a SurfaceTech GSA-X goniometer at 25 ℃ in air. The contact angle measurement was performed on a flat surface. The angles were measured immediately after dripping a water droplet on the surface of sample.

Synthetic Procedures

Synthesis of (*Z*)-2,3-bis(4-iodophenyl)acrylonitrile (2):

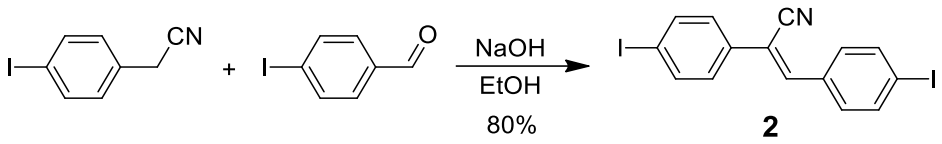

Scheme S1. Synthetic procedures for **2**.

A solution of NaOH (49.6 mg, 1.24 mmol, 0.12 equiv) in ethanol (30 mL) was added dropwise to the mixture of 4-iodophenylacetonitrile (2.43 g, 10 mmol, 1 equiv) and 4-iodobenzaldehyde (2.32 g, 10 mmol, 1 equiv) in ethanol (50 mL). The reaction mixture was stirred at rt for 1.5 h under nitrogen atmosphere. The resulting solid was filtered and sufficiently washed with cold ethanol. The desired product **2** was obtained as a white solid (4.08 g, 8.93 mmol, 89.3%). ^{1}H NMR ($CDCl_3$, 400 MHz): δ 7.39 (d, *J* = 8 Hz, 2 H), 7.44 (s, 1 H), 7.60 (d, *J* = 4 Hz, 2 H), 7.78 (d, *J* = 4 Hz, 2 H), 7.81 (d, *J* = 8 Hz, 2 H). The spectrum (Figure S17) matched with the reported data in S2.

Synthesis of (*Z*)-2,3-bis(4-bromophenyl)acrylonitrile (4):

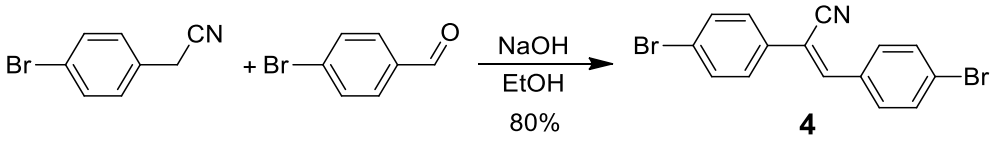

Scheme S2. Synthetic procedures for **4**.

A solution of NaOH (2.45 mg, 0.061 mmol, 0.12 equiv) in ethanol (1.5 mL) was added dropwise to the mixture of 4-bromophenylacetonitrile (100 mg, 0.51 mmol, 1 equiv) and 4-bromobenzaldehyde (94.38 mg, 0.51 mmol, 1 equiv) in ethanol (2.5 mL). The reaction mixture was stirred at rt for 1.5 h in nitrogen atmosphere. The solid was filtered and

sufficiently washed with cold ethanol. The desired product **4** was obtained as a white solid (100.3 mg, 0.28 mmol, 54.2%). ^{1}H NMR ($CDCl_3$, 400 MHz): δ 7.53 (d, *J* = 8 Hz, 2 H), 7.45 (s, 1 H), 7.58 (d, *J* = 8 Hz, 2 H), 7.60 (d, *J* = 8 Hz, 2 H), 7.74 (d, *J* = 12 Hz, 2 H). The spectrum (Figure S18) matched with the reported data in S3.

Synthesis of 7:

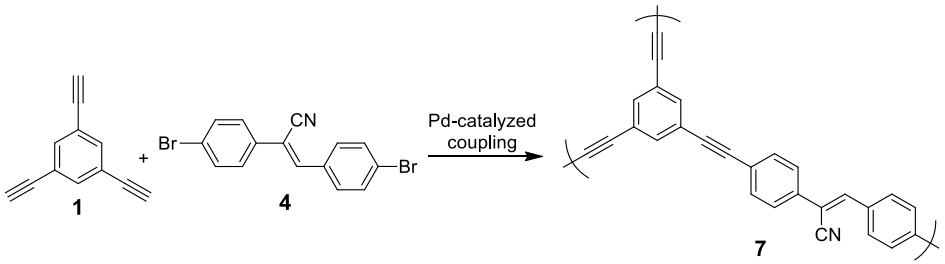

Scheme S3. Synthetic procedures for **7**.

Non-agitated reaction: To a solution of 1,3,5-triethynylbenzene (24.7 mg, 0.16 mmol, 1.0 equiv), (*Z*)-2,3-bis(4-bromophenyl)acrylonitrile (59.7 mg, 0.16 mmol, 1.0 equiv), and bis(triphenylphosphine)palladium(II) dichloride (3.46 mg, 4.9 μmol, 0.03 equiv) in toluene (1 mL) was added a solution of copper(I) iodide (0.94 mg, 4.9 μmol, 0.03 equiv) in triethylamine (0.5 mL). After storing at rt for 24 h without agitation, the resulting powder was filtered and washed with MeOH, THF, and acetone consecutively. The obtained product was further purified by gentle stirring in MeOH for 24 h and dried under vacuum at rt to afford **7** as a brown powder (8.52 mg, 10.1%). IR (cm^{-1}): 2970, 2155, 2109, 1739, 1577, 1435, 1367, 1217, 1095.

Agitated reaction: To a solution of 1,3,5-triethynylbenzene (74.0 mg, 0.49 mmol, 1.0 equiv), (*Z*)-2,3-bis(4-bromophenyl)acrylonitrile (178.8 mg, 0.49 mmol, 1.0 equiv), and bis(triphenylphosphine)palladium(II) dichloride (10.4 mg, 0.01 mmol, 0.03 equiv) in toluene (3 mL) was added a solution of copper(I) iodide (2.81 mg, 0.0148 mmol, 0.03 equiv)

in triethylamine (1.5 mL). After stirring at rt for 24 h, the resulting powder was filtered and washed with MeOH, THF, and acetone consecutively. The product was further purified by gentle stirring in MeOH for 24 h and dried under vacuum at rt to afford **7** as a brown powder (78.61 mg, 31.1 %).

Synthesis of 8:

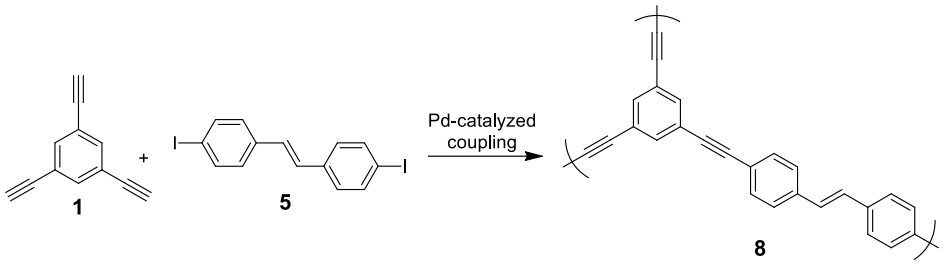

Scheme S4. Synthetic procedures for **8**.

1,3,5-Triethynylbenzene (49.4 mg, 0.33 mmol, 1.0 equiv), 4,4’-diiodo-*trans*-stilbene (0.14 g, 0.33 mmol, 1.0 equiv), and bis(triphenylphosphine)palladium(II) dichloride (6.92 mg, 0.0099 mmol, 0.03 equiv) were dissolved in 1:1 toluene–DMF (4 mL, v/v) after sonication. To the reaction mixture was added a solution of copper(I) iodide (1.88 mg, 9.9 μmol, 0.03 equiv) in triethylamine (1 mL). After storing at 85℃ for 24 h without agitation, the resulting product was taken out and washed with MeOH, THF, and acetone consecutively. The product was further purified by gentle stirring in MeOH for 24 h and dried under vacuum at rt to afford **8** as a dark brown powder (158.8 mg, 83%). IR (cm^{-1}): 3045, 2220, 1580, 1486, 1405, 1360, 1064, 1005.

Synthesis of 9:

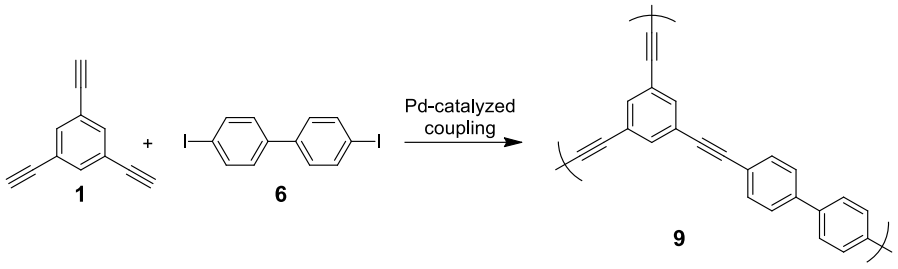

Scheme S5. Synthetic procedures for **9**.

1,3,5-Triethynylbenzene (24.7 mg, 0.16 mmol, 1.0 equiv), 4,4'-diiodobiphenyl (66.7 mg, 0.16 mmol, 1.0 equiv), and bis(triphenylphosphine)palladium(II) dichloride (3.46 mg, 0.0049 mmol, 0.03 equiv) were dissolved in toluene (1 mL) after sonication. Then, a solution of copper(I) iodide (0.94 mg, 4.9 μmol, 0.03 equiv) in triethylamine (0.5 mL) was added to the reaction mixture. After storing at 75℃ for 24 h without agitation, the resulting polymer was filtered and washed with MeOH, THF, and acetone consecutively. The product was further purified by gentle stirring in MeOH for 24 h and dried under vacuum at rt to afford **9** as a yellow powder (72.2 mg, 79%). IR (cm^{-1}): 2207, 1578, 1493, 1414, 1107, 1064, 1002. The resulting material **9** was obtained as a monolith but not compressible as shown in Figure S1.

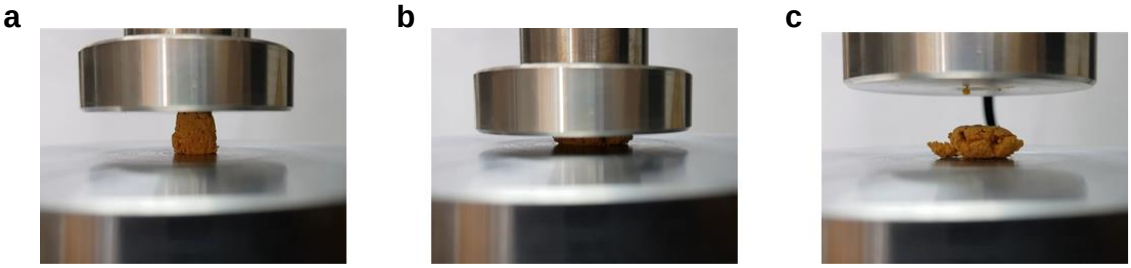

Figure S1. Photographs of the network **9** that was obtained as a monolith (a) but destroyed after (b) loading and (c) unloading external force.

Synthesis of 10:

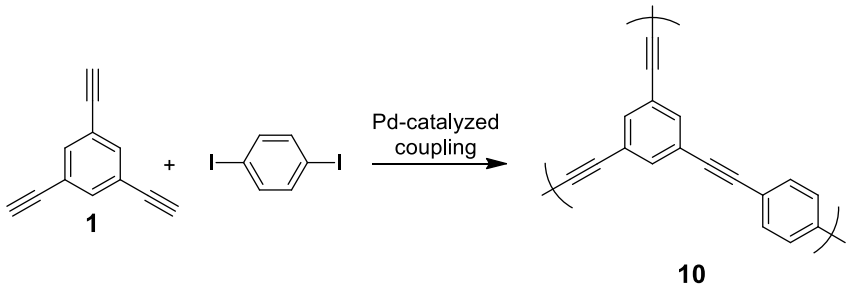

Scheme S6. Synthetic procedures for **10**.

Microporous polymer network **10** was prepared by following the reported procedure using 1,4-diiodobenzene instead of **2**.[S1] Quantities of monomers and reagents for **10**: 1,3,5-Triethynylbenzene (50 mg, 0.33 mmol, 1.0 equiv), 1,4-diiodobenzene (109.83 mg, 0.33 mmol, 1.0 equiv), bis(triphenylphosphine)palladium(II) dichloride (7.0 mg, 0.01 mmol, 0.03 equiv), and copper(I) iodide (2.0 mg, 0.01 mmol, 0.03 equiv). The product was obtained as a compressible, yellow monolith.

Mechanical Properties of 9

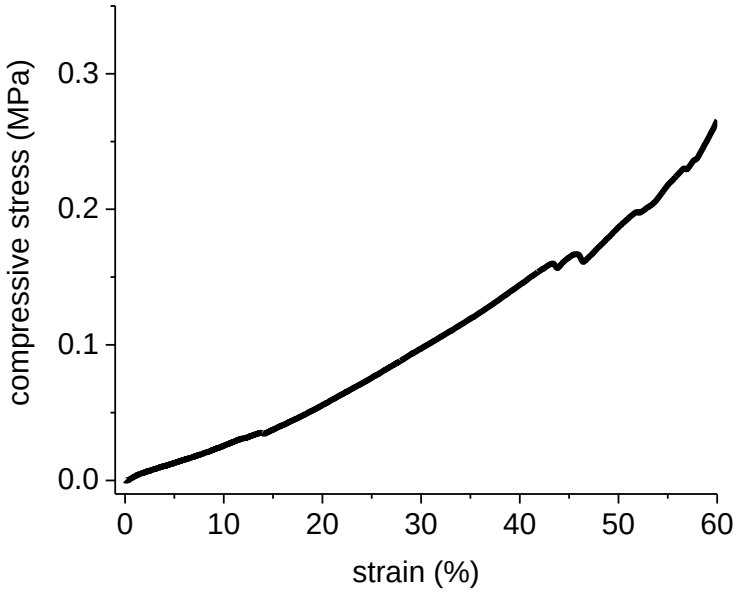

Figure S2. Compressive stress–strain curve obtained from **9**. The network was destroyed over a strain of 40%.

SEM Measurement

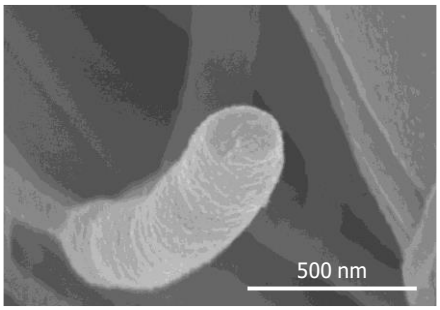

Figure S3. SEM image of the cross section of fiber in the network **3**.

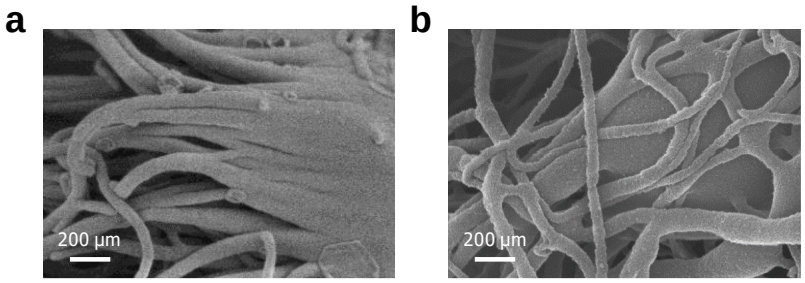

Figure S4. SEM images of fibrous structure in **3** (a) before and (b) after ten consecutive loading–unloading cycles.

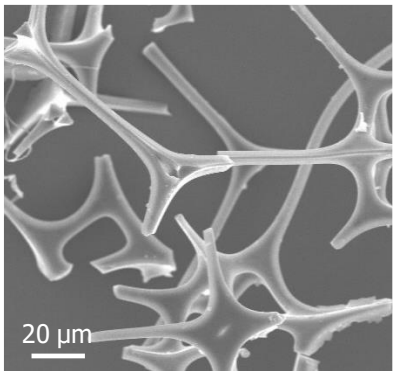

Figure S5. SEM image of fibrous structure of a commercial melamine foam.

Measurement of Porosity of Materials

Table S1. Summarized specific surface areas and total pore volumes of the polymer networks.

polymer network	specific surface area ($m^2\ g^{-1}$)[a]	total pore volume ($cm^3\ g^{-1}$)[b]
3	53	0.10
7	331	0.26
8	487	0.25
9	441	0.22

[a] specific surface areas were calculated by the BET method from N_2 adsorption isotherms at 77 K.
[b] total pore volume were determined at P/P_0 = 0.995.

Fiber Growth Measurement

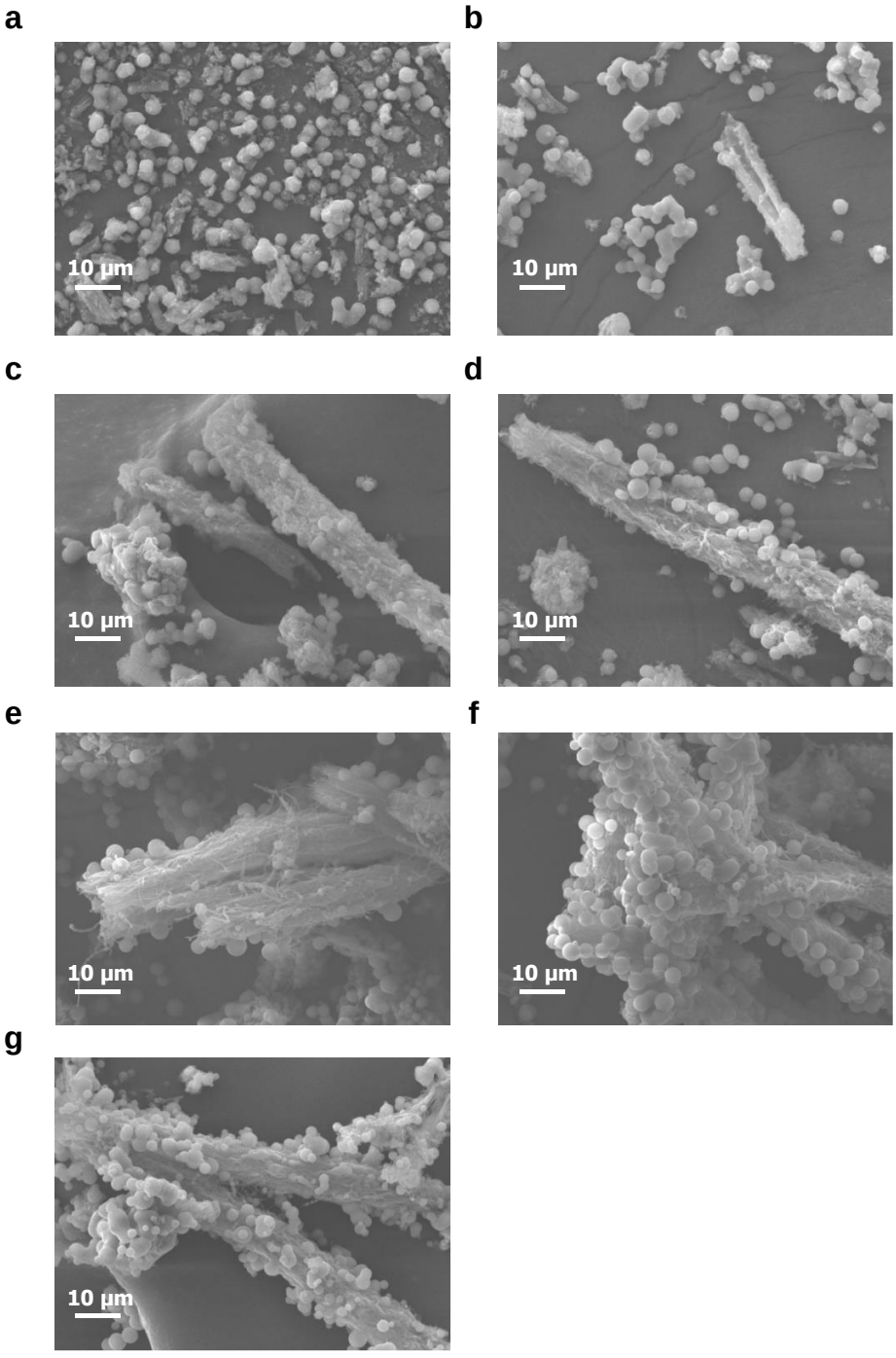

Figure S6. SEM images for the growth of fiber bundles during the synthesis of **3**, which were monitored at (a) 10, (b) 20, (c) 30, (d) 40, (e) 50, (f) 60, and (g) 120 min.

Mechanical Properties of Carbonized 3

The monolith **3** was carbonized following the conditions as follows. The material was heated up to 800 ℃ at a rate of 2 ℃ min^{-1} under nitrogen atmosphere. Then, the material was further stored at the same temperature for 1 h to complete the thermal carbonization (char yield, 80%).

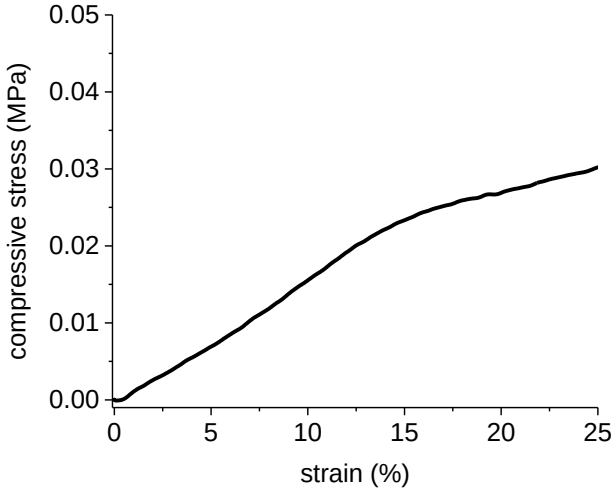

Figure S7. Compressive stress–strain curve obtained from the carbonized **3**. The network was destroyed over a strain of 15%.

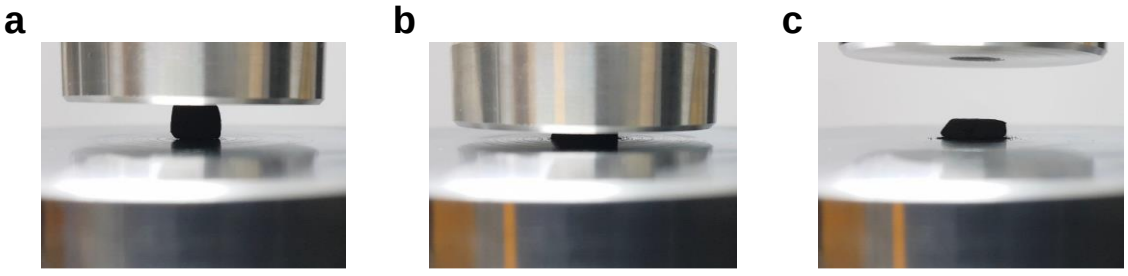

Figure S8. Photographs of the carbonized **3** that maintained the monolithic structure (a) but destroyed during (b) loading and (c) unloading cycle.

Optical Properties of 3

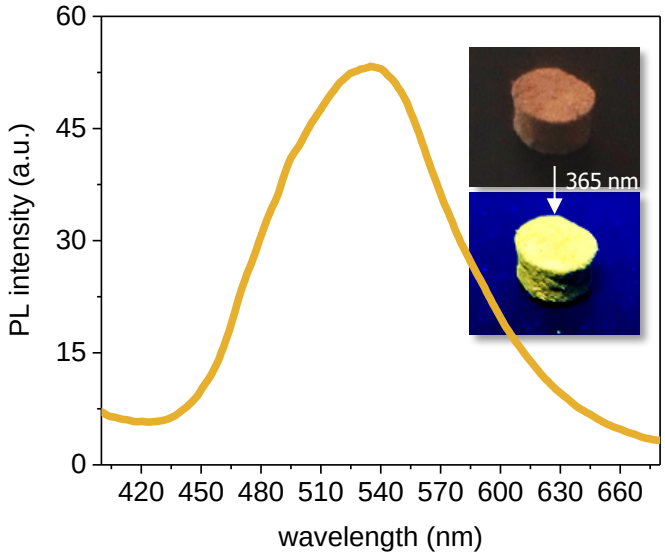

Figure S9. The fluorescence emission spectrum of **3** when excited at 365 nm (yellow). The inset shows photographs of **3** before and after 365-nm irradiation using a conventional UV hand lamp.

Contact Angle Measurement

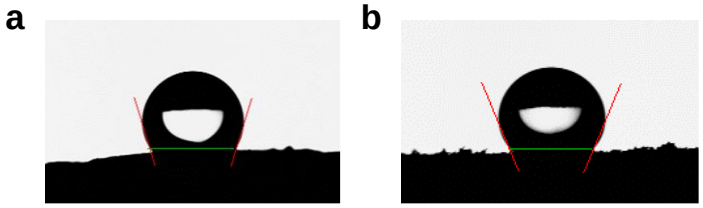

Figure S10. Representative photographs of a water droplet on polymer network **3** (a) before and (b) after ten consecutive loading–unloading cycles.

Table S2. Contact angles measured from polymer network **3**.

Compound	Trial 1	Trial 2	Trial 2	Avg.	Std.
3	107.82	101.94	93.18	100.98	7.37
3 after compressive test	108.49	111.34	106.93	108.92	2.24

Absorption Properties of Materials

Each dried sample was soaked in each solvent. Then the weight of samples was monitored at each time interval.

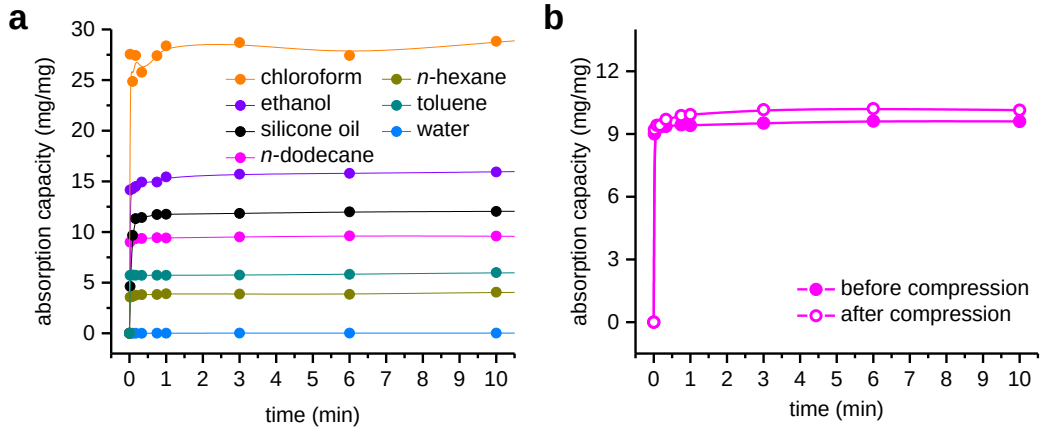

Figure S11. (a) Expanded view of the initial region of the absorption behavior of mesoporous **3**. The absorption almost completed before 10 min. (b) Comparison of the initial absorption behavior of **3** before (closed circles) and after compression until a strain of 80% (open circles) when immersed in *n*-dodecane.

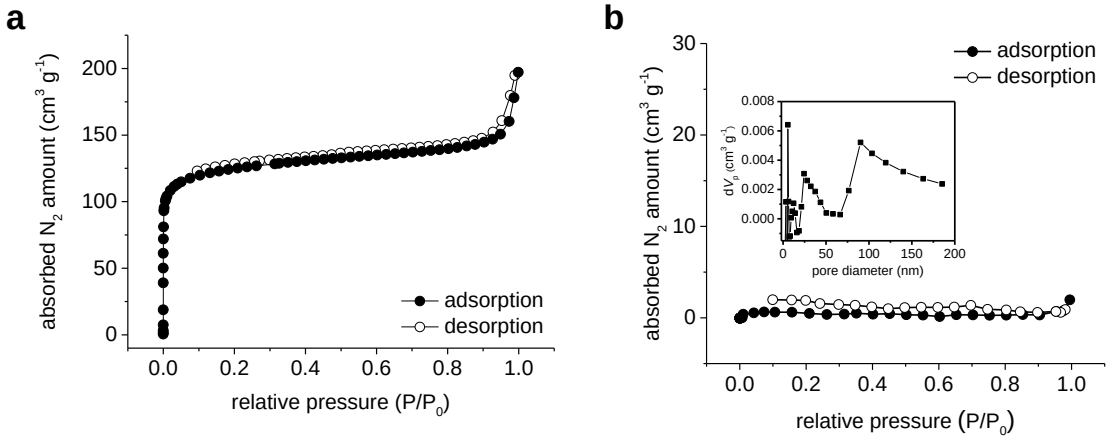

Figure S12. Nitrogen adsorption–desorption isotherms of (a) the network **10** and (b) melamine foam measured at 77 K. Open circles depict adsorption curves; closed circles, desorption curves. Pore size distribution of large pores in the melamine foam estimated by the Barrett–Joyner–Halenda (BJH) method is shown in the inset.

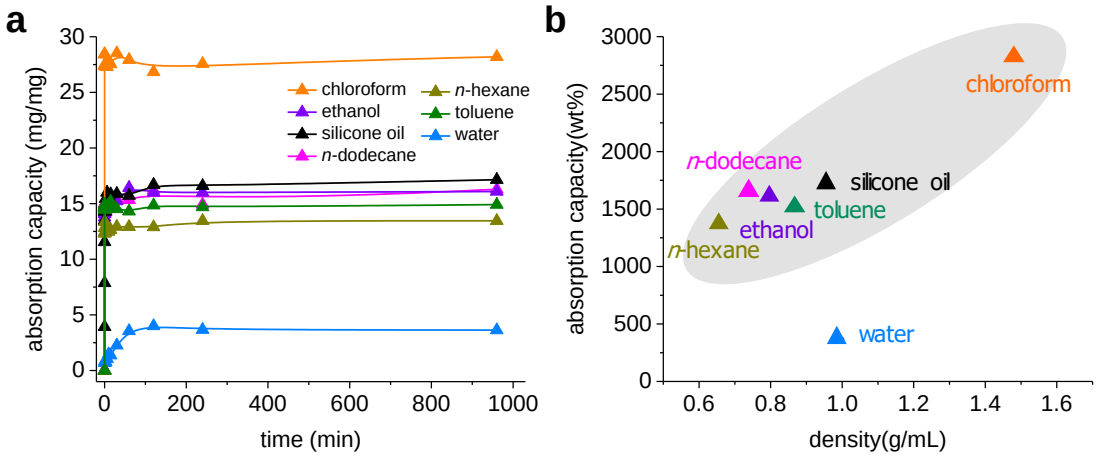

Figure S13. (a) Absorption behavior of microporous **10** when immersed in various solvents as a function of time. (b) Comparison of absorption capacity of **10** versus density of solvents.

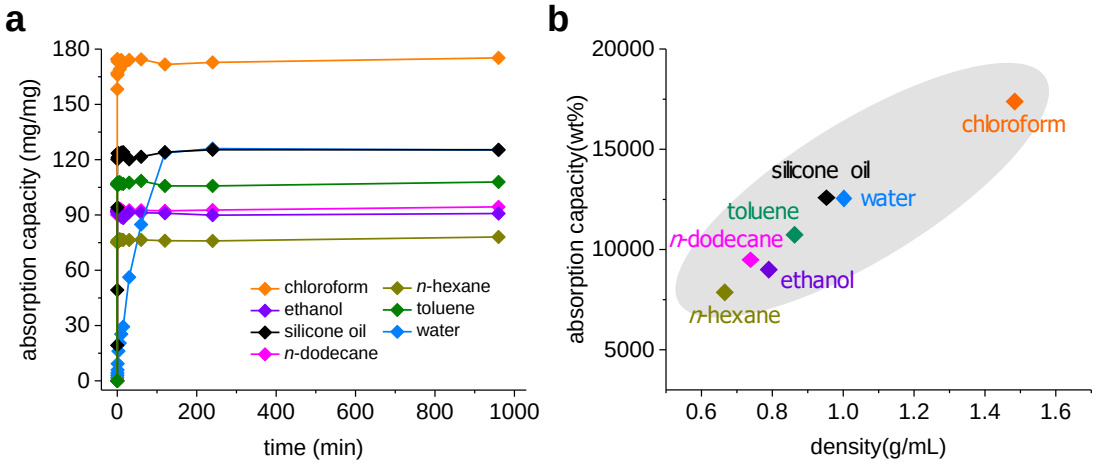

Figure S14. (a) Absorption behavior of melamine foam when immersed in various solvents as a function of time. (b) Comparison of absorption capacity of melamine foam versus density of solvents.

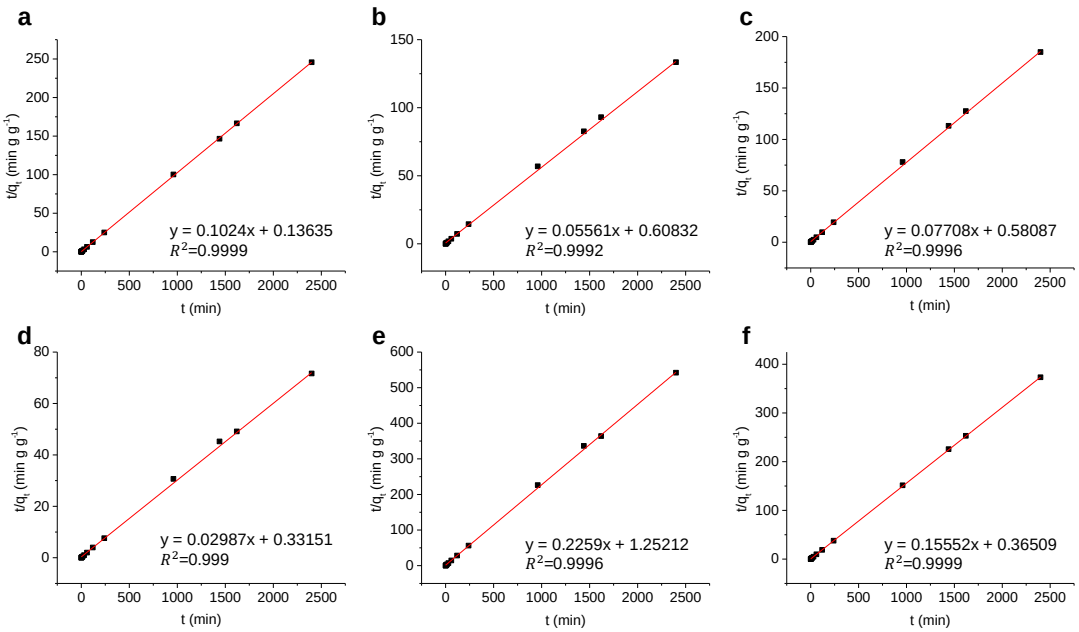

Figure S15. Linear correlation of t/q_t vs. time and obtained corresponding function for each solvent, measured with **3**: (a) *n*-dodecane, (b) ethanol, (c) silicone oil, (d) chloroform, (e) *n*-hexane, and (f) toluene.

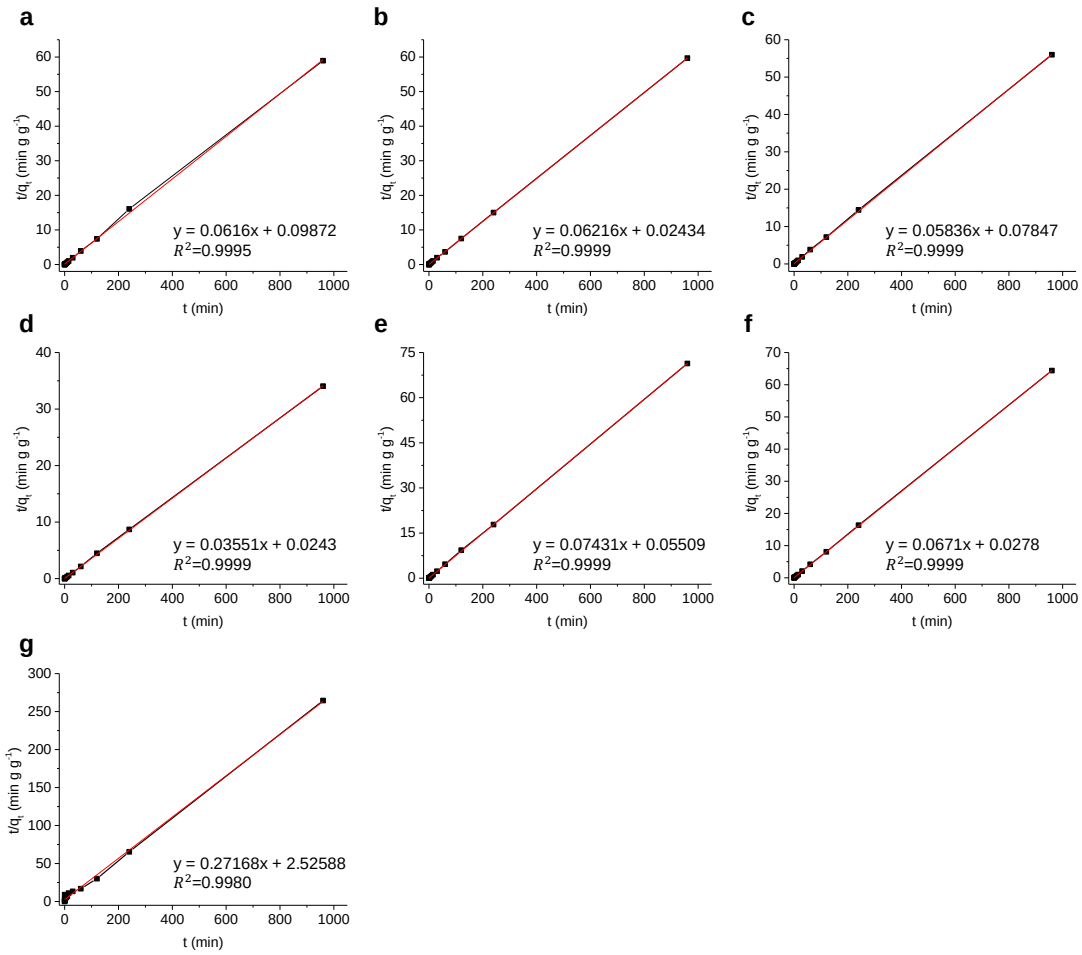

Figure S16. Linear correlation of t/q_t vs. time and obtained corresponding function for each solvent, measured with **10**: (a) *n*-dodecane, (b) ethanol, (c) silicone oil, (d) chloroform, (e) *n*-hexane, (f) toluene, and (g) water.

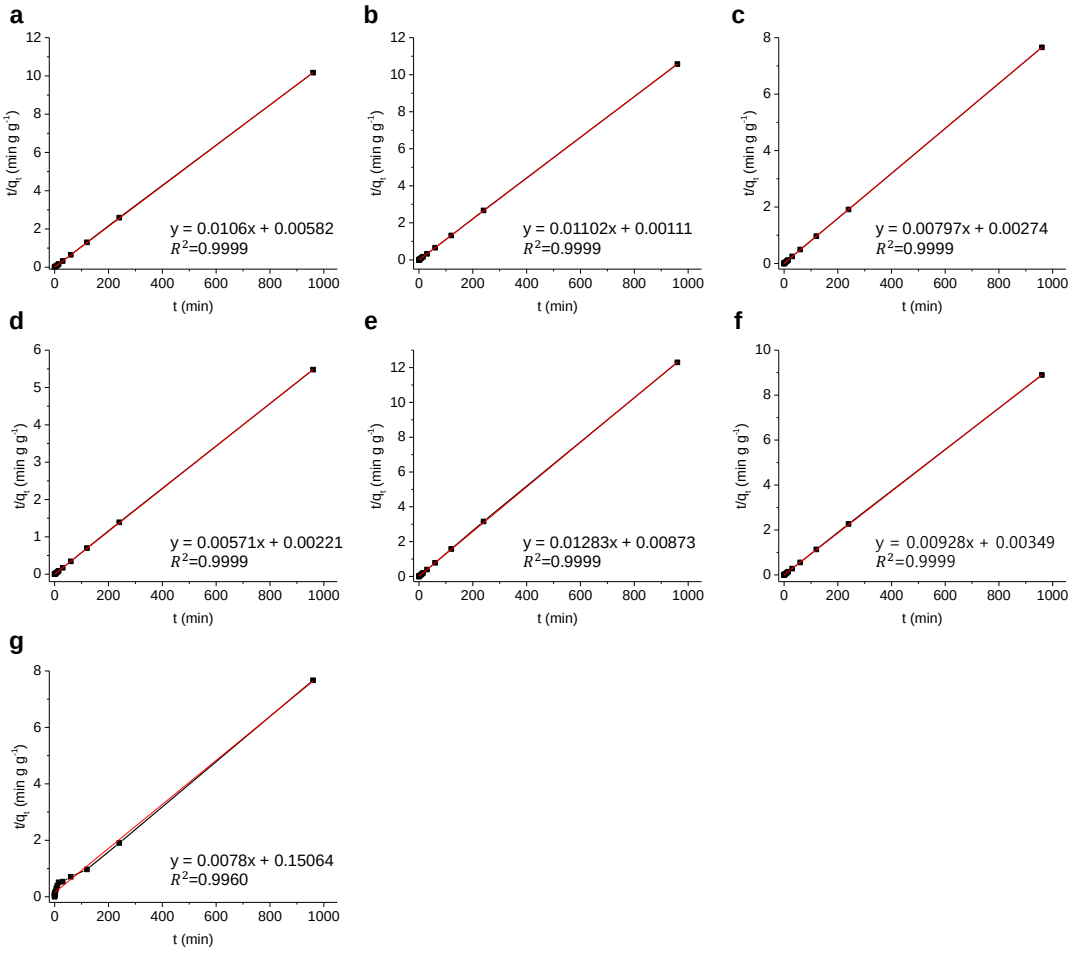

Figure S17. Linear correlation of t/q_t vs. time and obtained corresponding function for each solvent, measured with melamine foam: (a) *n*-dodecane, (b) ethanol, (c) silicone oil, (d) chloroform, (e) *n*-hexane, (f) toluene, and (g) water.

References

S1. Lee, K. M.; Kim, H. J.; Kang, C.-S.; Tojo, T.; Chae, J. A.; Oh, Y.; Cha, M. C.; Yang, K. S.; Kim, Y. A.; Kim, H. Preparation of carbon-containing, compressible, microporous, polymeric monoliths that regulate macroscopic conductivity. *Polym. Chem.* **2019**, *10*, 852–859.

S2. Chen, C.-H.; Lee, S.-L.; Lim, T.-S.; Chen, C.-h.; Luh, T.-Y. Influence of polymer conformations on the aggregation behaviour of alternating dialkylsilylene-[4,4′-divinyl(cyanostilbene)] copolymers. *Polym. Chem.* **2011**, *2*, 2850–2856.

S3. Upamali, K. A. N.; Estrada, L. A.; De, P. K.; Cai, X.; Krause, J. A.; Neckers, D. C. Carbazole-Based Cyano-Stilbene Highly Fluorescent Microcrystals. *Langmuir* **2011**, *27*, 1573–1580.

NMR Spectra

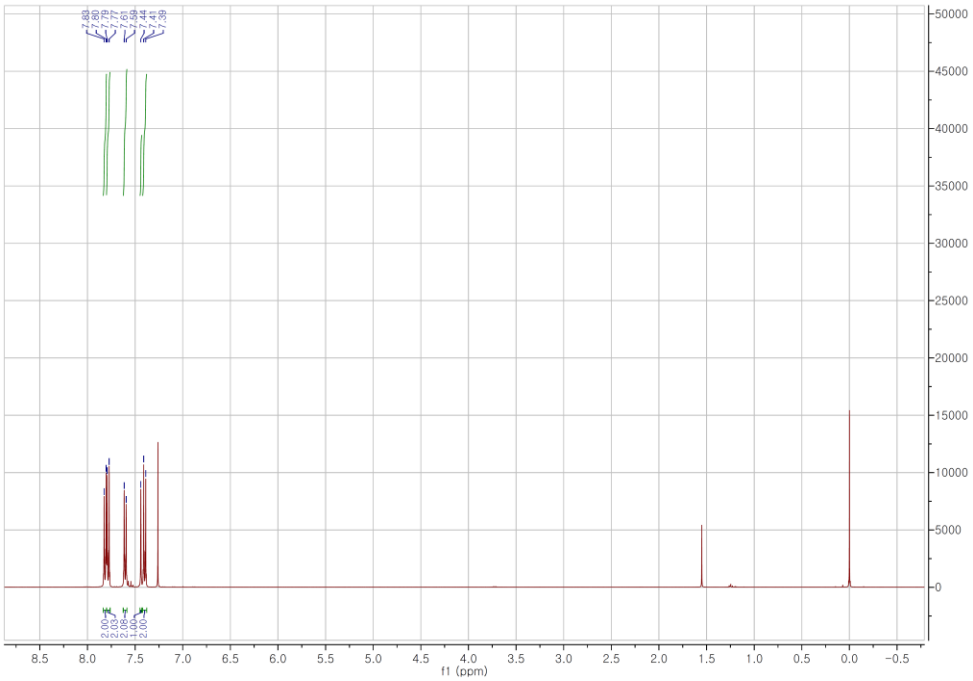

Figure S18. ^{1}H NMR spectrum of **2**.

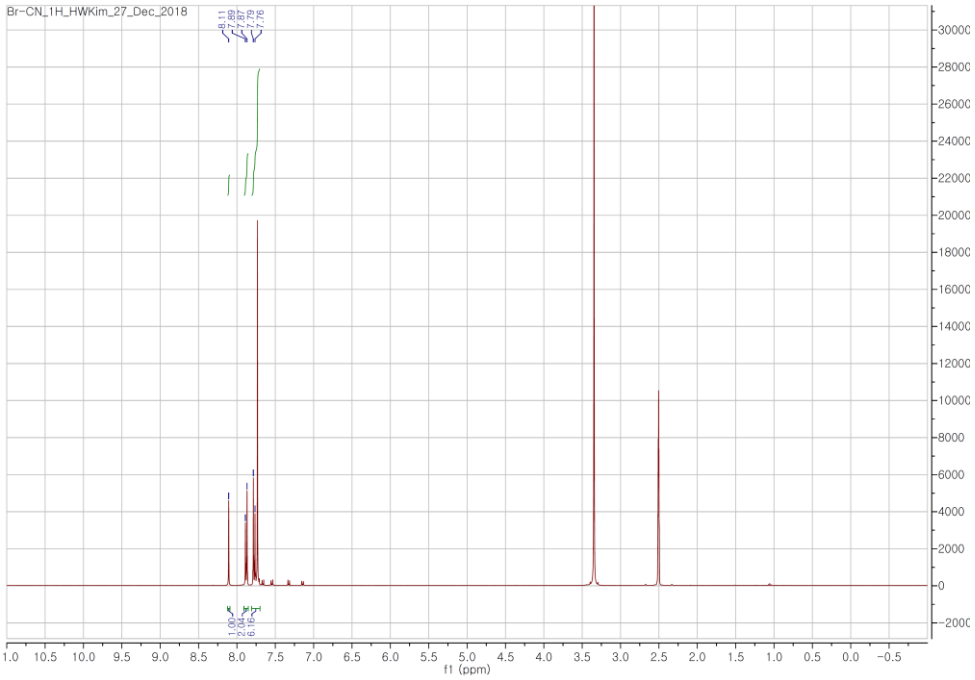

Figure S19. ^{1}H NMR spectrum of **4**.